3-D Simulation of Interdigitated-Back-Contact Silicon Solar Cells With Quokka Including Perimeter Losses

Andreas Fell, Kean C. Fong, Keith R. McIntosh, Evan Franklin, and Andrew W. Blakers

***Abstract*—An interdigitated-back-contact (IBC) version of Quokka, a recently developed free and fast solar cell simulation program, is presented. It is capable of simulating IBC unit cells with a variety of interdigitated contact and diffusion patterns in both 2-D and 3-D. The program is evaluated by comparing simulated and experimental current–voltage (*I–V*) curves of high-efficiency IBC solar cells. The simulations include the perimeter effects of edges and busbars by simulating the inner unit cell in 3-D, and accounting for the edges and busbars by 2-D unit cell approximations. The simulation agrees well with the experiment under 1-sun conditions with different aperture areas. Furthermore, simulations of the inner unit cell are successfully validated against Sentaurus Device, for both the *I–V* curve and detailed free energy losses at maximum power point. The results evidence the validity of the quasi-neutral and conductive-boundary approximations employed by Quokka for fast simulation of IBC solar cells.**

***Index Terms*—Busbar losses, free energy loss analysis (FELA), interdigitated-back-contact (IBC), loss analysis, modeling, perimeter losses, quokka, simulation, solar cell.**

I. Introduction

On the route to increasing efficiencies of laboratory and industrial silicon solar cells, more complex cell designs are increasingly under consideration, in particular the incorporation of localized features. This increase in the degrees of freedom motivates comprehensive modeling for gaining understanding and optimizing the cell design. Access to suitable multidimensional device simulation software is still limited. While the state-of-the-art device simulators Sentaurus and Atlas are very powerful, their drawbacks are computation time, complexity of setup, and price.

A computationally less expensive device model can be derived by using the quasi-neutrality assumption and/or conductive boundary conditions [1], [2]. The latter comes with the practically significant advantage of requiring input values for the surface diffusions more easily derived from experiments, that is the sheet resistance and the recombination current prefactor J_0, rather than the diffusion profile and the surface recombination velocity. Free implementations of such a model exist with QSS model [3]–[5], which is essentially 1-D with some semianalytical multidimensional features, CoBoGUI [2], which requires a Comsol license, and PC2D [6], which comes with low speed and inflexible meshing, both of the latter two are currently restricted to 2-D. Recently, Quokka was released for free on pvlighthouse.com.au [1], [7], featuring fast and easy to set up unit cell simulations in 1-D/2-D/3-D.

An approach to model a full-size solar cell including perimeter losses, based on multiple unit cell simulations combined with a distributed electrical network model, was presented in [8] for a 3-D device structure. So far publications on numerical simulation of interdigitated-back-contact (IBC) solar cells are restricted to 2-D, using mostly Sentaurus Device [9]–[11]. Sunpower did use Atlas and an in-house 2-D quasi-neutral conductive-boundary model for IBC cell simulation [12]. More recently, CoBoGUI was used [13], [14], in the latter case including a distributed network simulation to account for the distributed grid resistance. Quokka was used in [15] for optimization of a 3-D IBC unit cell design reaching 24.4% efficiency [16]. Perimeter losses of IBC cells have been modeled analytically in [17], but have not been published yet using numerical device simulation.

This paper describes the IBC version of Quokka, capable of simulating a 2-D/3-D unit cell with a variety of interdigitated contact and diffusion patterns. To validate the Quokka IBC version, simulation results are compared with experimental current–voltage (*I–V*) curves of high-efficiency IBC cells, as well as with Sentaurus Device. Particular attention is given to perimeter losses, which for the small cells under investigation are significant, and thus must be accounted for when making a quantitative comparison with measurements. Those perimeter effects are considered by simulating the inner 3-D unit cell, as well as representative 2-D approximations of the busbar and finger edge regions, which is equivalent to the approach presented in [8].

As an extension to Quokka, the incorporation of the free energy loss analysis (FELA) is described, enabling a quick detailed loss analysis of the cell performance, e.g., at the maximum power point (MPP), with the same units (dissipated power per unit area) for resistive and recombinative loss contributions.

Manuscript received April 23, 2013; revised April 10, 2014; accepted April 16, 2014. Date of publication May 8, 2014; date of current version June 18, 2014. This work was supported by the Australian Solar Institute/Australian Renewable Energy Agency under the fellowship 5-F007.

A. Fell, K. C. Fong, E. Franklin, and A. W. Blakers are with the College of Engineering and Computer Science, Australian National University, Canberra, A.C.T. 0200, Australia (e-mail: andreas.fell@anu.edu.au; kean.fong@anu.edu.au; evan.franklin@anu.edu.au; andrew.blakers@anu.edu.au).

K. R. McIntosh is with the PV Lighthouse, Wollongong, N.S.W. 2500, Australia (e-mail: krmcintosh@pvlighthouse.com.au).

Color versions of one or more of the figures in this paper are available online at http://ieeexplore.ieee.org.

Digital Object Identifier 10.1109/JPHOTOV.2014.2320302

II. Quokka Model Extensions

A. Free Energy Loss Analysis

As an extension to the models presented in [1], FELA as described in [18] is implemented. In addition to the presented contributions, the power loss at the contact resistance $\dot{f}_{\mathrm{res,cont}}$ is considered by the following integral over the contacted boundary $\delta V, \mathrm{cont}$, which accounts correctly for the spatial variation due to current transfer effects

$$\dot{f}_{\mathrm{res,cont}} = A^{-1} \int\limits_{\delta V,\mathrm{cont}} dA \left(\varphi_{\mathrm{diff}} - V_{\mathrm{uc}}\right)^2 / r_{\mathrm{c}}. \tag{1}$$

Here, A denotes the unit cell area, φ_{diff} the majority carrier quasi Fermi potential in the conductive boundary, V_{uc} the voltage applied to the unit cell boundary (not at the terminal, i.e., excluding external circuit elements), and r_c the contact resistivity. Losses at the external shunt and series resistivity r_{shunt} and r_{series} are calculated with the total current density of the unit cell J_{uc}

$$\dot{f}_{\mathrm{res,shunt}} = V_{\mathrm{uc}}^2 / r_{\mathrm{shunt}} \tag{2}$$

$$\dot{f}_{\mathrm{res,series}} = \left(J_{\mathrm{uc}} - V_{\mathrm{uc}}/r_{\mathrm{shunt}}\right)^2 r_{\mathrm{series}} = J_{\mathrm{term}}^2 r_{\mathrm{series}}. \tag{3}$$

The sum of the resistive losses $\dot{f}_{\mathrm{res}}$, recombinative losses $\dot{f}_{\mathrm{rec}}$, and the terminal power density $\dot{f}_{\mathrm{term}} = V_{\mathrm{term}} J_{\mathrm{term}}$ must be equal to the generated power density $\dot{f}_{\mathrm{gen}}$. The amount of deviation of this balance gives a metric for the solution accuracy $\varepsilon_{\mathrm{FELA}}$, which we define as

$$\varepsilon_{\mathrm{FELA}} = \left(\dot{f}_{\mathrm{gen}} - \dot{f}_{\mathrm{res}} - \dot{f}_{\mathrm{rec}} - \dot{f}_{\mathrm{term}}\right) / \max(\dot{f}_{\mathrm{gen}}, \dot{f}_{\mathrm{term}}). \tag{4}$$

Note that while this error gives a useful indication of the overall numerical error, a low value is not sufficient evidence of an accurate solution since the balance can possibly still yield a low value despite, for example, a coarse and thus inaccurate discretization being used. Throughout this study, a high overall numerical accuracy is ensured by checking both mesh independence and a low $\varepsilon_{\mathrm{FELA}}$.

B. Interdigitated-Back-Contact Extension

A key feature for the IBC version is a flexible 2-D/3-D meshing algorithm accepting a set of input parameters to generate a variety of different diffusion and contact patterns with user defined dimensions.

To account for the different optical properties of the different rear surfaces, Quokka IBC optionally accepts different generation profiles for each of the different regions, i.e., junction/base/undiffused, contacted/noncontacted, and metallized/nonmetallized, which we call generation profile splitting. To distinguish the latter one, the half-width of the metal fingers has to be defined. However, it is not electrically considered, i.e., no shunting occurs if one metal finger covers surface regions of different polarities.

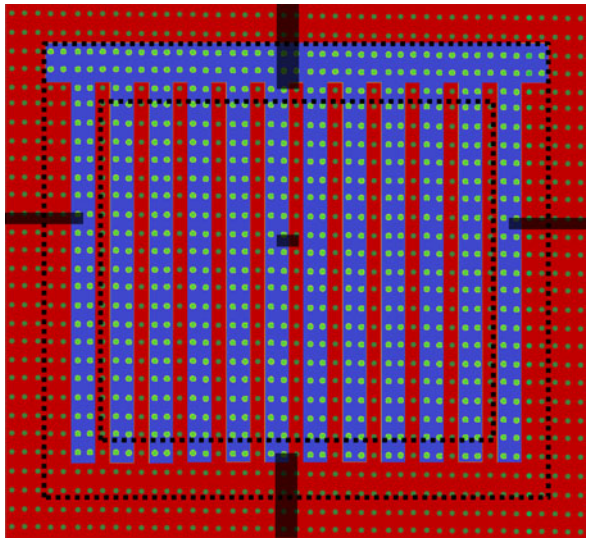

Fig. 1. Rear view of the cell layout (not to scale). *Red*: n-type (base) diffusion, *blue*: p-type (emitter) diffusion, *green*: regular pattern of dot contact openings. Dashed lines show the illuminated area for the 16- and 12.96-cm^2 aperture, respectively. Shaded rectangles highlight the different unit cell regions to be simulated, comprising the inner unit cell, n-busbar, p-busbar, and finger edge regions. Not shown is the metal layer, which is aligned to the diffusion pattern and restricted to the 16-cm^2 area.

III. Simulation Setup

A. Multiple Unit Cell Approach

A sketch of the IBC cell layout is given in Fig. 1. Rather than restricting the simulation to the inner unit cell, we include the effects of the busbar and finger edge losses by several different unit cell simulations, that is, using additional dedicated unit cells corresponding to the busbars regions and the regions next to the finger edges. Such an approach thus fully considers carrier flow to and recombination (both in the bulk and at front and rear surfaces) within each of the cell's perimeter regions. The inherent assumption that no carrier diffusion occurs between the inner unit cell and the edge unit cells is valid provided that the unit cell boundary voltages are identical, which is the case for low contact and metal grid resistance.

In Fig. 2, the geometries of the individual unit cells are shown. A few assumptions and simplifications are imposed to ease the setup of the simulation within the standard settings of Quokka.

1) For the inner unit cell, the circular contacts are approximated by square ones with the same area for more efficient meshing and simulation speed.
2) The busbar and edge regions are approximated by 2-D unit cells where the contacted area is treated homogenously with the contact resistivity and J_0 values being area-averaged according to the contact fraction. This is a valid approximation as it was found that in this particular cell design resistive losses in the diffusions are negligible.
3) The n-diffused, noncontacted region outside of the cell area is represented by a width of 1 mm to the solution domain boundary, as any greater value has been found to not change the results.

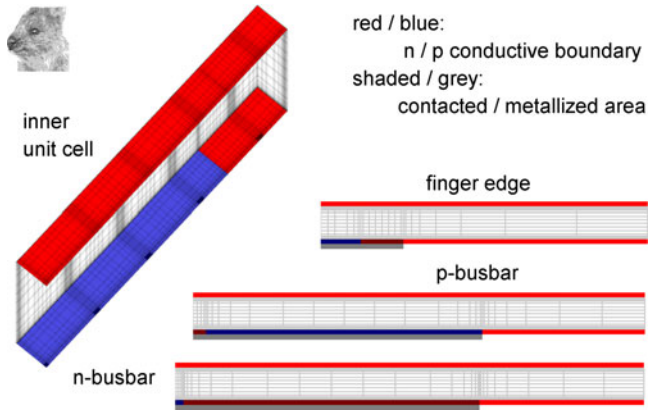

Fig. 2. Unit cell geometries as produced by Quokka, comprising the inner 3-D unit cell and simplified 2-D unit cells for the busbar and finger edge regions; grey lines indicate the metal coverage used to split the generation profile.

For each unit cell, we simulate the dark and light *I–V* curve, where for the perimeter regions generation profile splitting is applied in such a way that zero generation is achieved outside of the cell area. In addition, note that for the busbar simulations the grid resistance is excluded.

The simulated current densities at a given terminal voltage are then averaged, weighted by the area of the individual regions, as described in (5)–(7), where A denotes the part of the area represented by the respective unit cell. It should be noted that the total area weighting of the inner unit cell is fractionally reduced to accommodate the busbar and edge unit cells, which are required to reach slightly into the inner cell area to have contacts of both polarities, as illustrated in Fig. 1. This area weighted averaging approach is equivalent to a parallel connection of the individual regions while neglecting the influence of the distributed nature of the metal grid resistance, which is a reasonable assumption considering the relatively small cell area investigated. Note that for the smaller aperture light *I–V* curves, the edge regions and part of the inner cell area are in dark conditions

$$J^{\mathrm{dark}} = \Big[A_{\mathrm{inner}} J^{\mathrm{dark}}_{\mathrm{inner}} + A_{\mathrm{nbus}} J^{\mathrm{dark}}_{\mathrm{nbus}} + A_{\mathrm{pbus}} J^{\mathrm{dark}}_{\mathrm{pbus}} + A_{\mathrm{edge}} J^{\mathrm{dark}}_{\mathrm{edge}}\Big] / 16\ \mathrm{cm}^2 \quad (5)$$

$$J^{\mathrm{light}}_{12.96\,\mathrm{cm}^2} = \Big[A^{\mathrm{light}}_{\mathrm{inner}} J^{\mathrm{light}}_{\mathrm{inner}} + A^{\mathrm{dark}}_{\mathrm{inner}} J^{\mathrm{dark}}_{\mathrm{inner}} + A_{\mathrm{nbus}} J^{\mathrm{dark}}_{\mathrm{nbus}} + A_{\mathrm{pbus}} J^{\mathrm{dark}}_{\mathrm{pbus}} + A_{\mathrm{edge}} J^{\mathrm{dark}}_{\mathrm{edge}}\Big] / 12.96\ \mathrm{cm}^2 \quad (6)$$

$$J^{\mathrm{light}}_{16\,\mathrm{cm}^2} = \Big[A_{\mathrm{inner}} J^{\mathrm{light}}_{\mathrm{inner}} + A_{\mathrm{nbus}} J^{\mathrm{light}}_{\mathrm{nbus}} + A_{\mathrm{pbus}} J^{\mathrm{light}}_{\mathrm{pbus}} + A_{\mathrm{edge}} J^{\mathrm{light}}_{\mathrm{edge}}\Big] / 16\ \mathrm{cm}^2. \quad (7)$$

B. Device Properties

The experimental cells to be simulated are IBC cells produced at the ANU reaching efficiencies of 22.6%. Details on this batch can be found in [19] and [20].

All input parameters needed for the simulations have been derived from direct measurements, test structures, or calculations [15]. It is important to note that we do not incorporate the uncertainty of the experimentally derived parameters for fitting the simulation results. An overview of the used parameter values is given in Table I.

TABLE I
PARAMETERS USED IN THE SIMULATIONS

name	value
cell thickness	190 µm
emitter diffusion half width	245 µm
base diffusion half width	80 µm
contact radius	3.5 µm
contact pitch (x and y)	70 µm
busbar width	1800 µm
n-type bulk resistivity	0.93 Ωcm
SRH electron lifetime	4 ms
SRH hole lifetime	4 ms
emitter diffusion sheet resistance	58 Ω/□
base diffusion sheet resistance	32 Ω/□
n-type front diffusion sheet resistance	240 Ω/□
emitter diffusion J_0 – passivated[1]	88.8 fA/cm^2
emitter diffusion J_0 - contacted[1]	1020 fA/cm^2
base diffusion J_0 - passivated[1]	142 fA/cm^2
base diffusion J_0 - contacted[1]	497 fA/cm^2
front diffusion J_0[1]	16.8 fA/cm^2
emitter contact resistance[2]	<1e^{-6} Ωcm^2
base contact resistance[2]	1e^{-4} Ωcm^2
external series resistance[3]	0.38 Ωcm^2
assumed effective intrinsic carrier density $n_{i,\mathrm{eff}}$[4]	9.65e^9 cm^{-3}

[1]Derived from symmetric QSSPC samples
[a]Derived from transfer length method (TLM) test structures
[3]Metal grid resistance calculated as described in the text
[4]consistently used for both the J_0 derivation and the simulation

The value for the metal grid resistance was calculated from the measured geometry of the metal grid, the conductivity of pure Al, and the measured height of the Al grid (3.0 μm). The calculations followed an analytical procedure and assumed that the current collection along each finger led to a linearly increasing current.

To determine the generation profile, we applied OPAL2 [21]. This was achieved by first measuring the wavelength-dependent complex refractive indexes $[n(\lambda)$ and $k(\lambda)]$ of the SiN_x and SiO_2 films that were deposited and grown on the front surface of the cell. Then, the thicknesses of these films were first set such that the hemispherical reflection calculated by OPAL 2 for ideal random upright pyramids fit the experimental reflection. Next, an effective path length enhancement of $Z = 6$ was assumed based on ray tracing of similar structures [22] accounting for suboptimal internal reflection at the rear and free-carrier absorption. And finally, by loading these inputs in OPAL2, the generation profiles were calculated for the unpolarized AM1.5g spectrum under normally incident light.

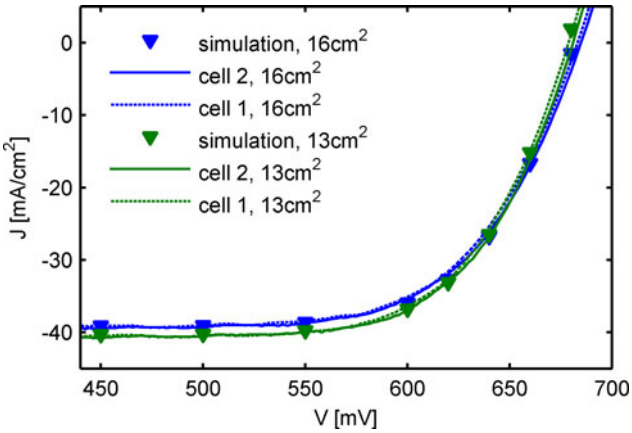

Fig. 3. Simulated and experimental light *I–V* curves for the different aperture sizes.

TABLE II
LIGHT *I–V* CURVE DATA FOR DIFFERENT APERTURE SIZES

	V_{oc} [mV]	J_{sc} [mA/cm^2]	FF [%]	η [%]
simulation *12.96 cm^2*	679	40.3	80.7	22.1
simulation *16 cm^2*	681	39.1	80.4	21.4
cell 1 *12.96 cm^2*	681	40.9	81.0	22.6
cell 1 *16 cm^2*	685	39.5	80.5	21.7
cell 2 *12.96 cm^2*	679	40.6	81.5	22.5
cell 2 *16 cm^2*	683	39.3	80.6	21.6
simulation *difference*	**-2.8**	**1.2**	0.3	0.7
cell 1 *difference*	**-3.8**	**1.4**	0.5	0.8
cell 2 *difference*	**-4.5**	**1.4**	0.9	0.8

IV. RESULTS AND DISCUSSION

A. Light I–V Curve Comparison

In Fig. 3 and Table II, the light *I–V* curves of the simulation results and of the two best experimental cells from the investigated batch are shown, for both fully illuminated (16 cm^2) and apertured (13 cm^2) measurements, and demonstrate an overall good agreement. In particular, the difference in V_{oc} and J_{sc} between the two aperture sizes, which can be expected to exclude most of the systematic error of the simulation input parameters and measurement setup, agree well within the experimental accuracy. This evidences an accurate modeling of the perimeter losses by the presented approach.

Likely causes for the slight understatement in V_{oc} in the simulation are experimental errors and deviations in the J_0 of the test structures compared with the actual cell properties, and more so, in the SRH bulk lifetime. The deviation of J_{sc} is most likely to be caused by an error in intensity of the solar simulator illumination, which is estimated at $\pm$ 2%.

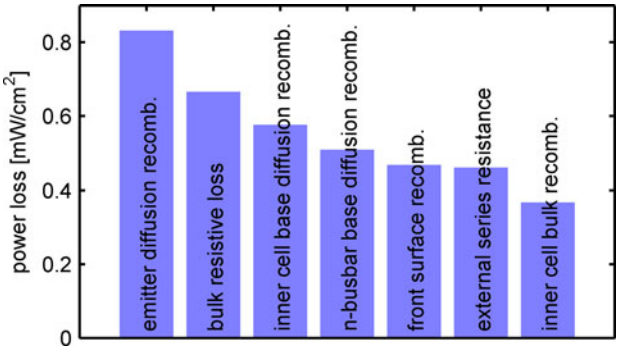

Fig. 4. FELA results of the 16-cm^2 aperture illumination at MPP with the individual unit cell results normalized to the total cell area. Shown are the first seven largest contributions only.

The difference between simulated and measured fill factors (FFs) appears, however, too large to be solely explained by experimental inaccuracies. Possible reasons for the understatement of the FF and its deviation are: 1) an injection dependence of the J_0 values caused, for example, by surface charge on the light front diffusion and 2) other nonideal recombination extending to MPP voltages and thus reducing FF [23]. Significant and largely different nonideality is revealed by dark *I–V* measurements of the two cells (not shown), and might cause the deviation and large scatter of the FF values. In similarly fabricated cells, this has been linked to the Al spiking through the p+ emitter in small isolated locations and creating Schottky contacts to the n-type bulk.

B. Free Energy Loss Analysis and Sentaurus Device Validation

We utilize the FELA output data to present a detailed loss analysis of the investigated cells at MPP. For this, the power loss contributions of the individual unit cells are area-averaged equivalents of the current densities in (5)–(7). This results in comparable values in power per cell area [mW/cm^2] for all loss contributions. In Fig. 4, the seven largest individual loss contributions are shown for the 16-cm^2 aperture illumination at MPP. Recombination at the emitter diffusion is identified as the major limit for the efficiency. The importance of recombination at the edges and busbars is also apparent, in particular the recombination at the base diffusion of the n-type busbar, an effect well known as "electrical shading."

To further validate the Quokka IBC version, we implement the identical inner unit cell geometry in Sentaurus Device. For the diffused regions, we use EDNA2 [24] to derive doping profiles which yield the J_0 values and sheet resistances quoted in Table I. For improved accuracy, we then extract the J_0 values from a dark simulation run in Sentaurus as described in [25] as inputs for Quokka. To ensure identical generation, profiles are used when comparing both device simulation tools; Quokka is rerun using the exact generation profile as created by Sentaurus. We further ensure identical models for $n_{i_{eff}}$, intrinsic recombination and carrier mobility in the bulk.

Comparison of the light *I–V* curve between Sentaurus and Quokka results in a very low overall deviation of $<0.2\%$, including the *I–V* curve parameters V_{oc}, J_{sc}, and FF, which is in

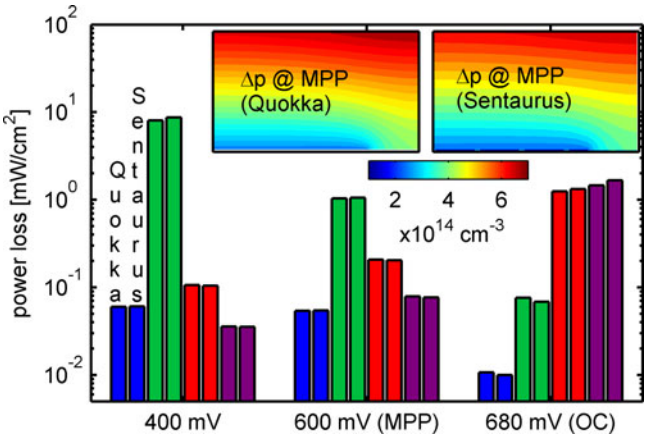

Fig. 5. Comparison of Sentaurus with Quokka simulation results at three different terminal voltages; the bars show groups of Quokka/Sentaurus pairs of bulk FELA contributions: electron transport loss (first pair *blue*), hole transport loss (second pair *green*), SRH recombination (third pair *red*), and Auger recombination (last pair *violet*); insert shows excess carrier densities Δp at MPP at the cross section through the contact centers.

the order of what can be expected to be the residual numerical error of both simulation tools. Furthermore, we extract spatial solution data at three terminal voltages, namely 400 mV, (close to $J_{\rm sc}$), 600 mV (MPP), and 680 mV ($V_{\rm oc}$). Within MATLAB, we then perform the FELA for the bulk region only, which is the solution domain of Quokka. The results are compared in Fig. 5 together with a plot of excess carrier density at MPP for an identical 2-D cross section of the unit cell. The very good agreement between Sentaurus and Quokka, both for this loss breakdown over two orders of magnitude and for the spatial distribution, evidences further the validity of the model assumptions and the accurate implementation of silicon IBC cells within Quokka. The simulation time for the *I–V* curve was several minutes in Quokka on a single processor compared with several hours to days dependent on mesh settings in Sentaurus on four processors, showing the vast speed advantage of Quokka for cell designs where the underlying model assumptions are valid.

V. Conclusion

We presented the successful implementation of an IBC version in Quokka. It allows for a variety of different contact and diffusion patterns and is thus suitable for most common IBC unit cell designs. To account for different rear reflectivities, Quokka accepts multiple generation profiles for different regions. Furthermore, the FELA is implemented in Quokka, providing a full quantitative loss analysis of both resistive and recombinative losses after each simulation.

Perimeter losses of the investigated IBC cell, that is losses at the busbar and finger edge regions, as well as effects because of different illumination aperture sizes, are considered by approximating the perimeter regions by 2-D unit cells in addition to the 3-D inner unit cell, and by then area averaging the dark and light *I–V* curves. The experimental and simulated light *I–V* curves match well within the experimental error, in particular the differences between the two applied aperture sizes. Furthermore, we validate Quokka by a careful comparison to the state-of-the-art device simulator Sentaurus device, which resulted in an excellent agreement ($\ll$1% for all relevant simulation results) within the order of the expected numerical inaccuracies. This supports the validity of the quasi-neutral and conductive-boundary approximations for simulations of IBC cells and its accurate implementation in Quokka.

Given the fast simulation speed even in 3-D compared with alternative more sophisticated tools (e.g., Sentaurus) and the relatively low effort in simulation setup, the IBC version of Quokka provides an attractive tool for loss analysis and extensive optimization of 2-D/3-D IBC silicon solar cell designs.

Acknowledgment

The authors would like to thank S. Zin and T. Choon for fabrication of the investigated solar cells within a project funded by the Solar Energy Research Institute of Singapore, and the joint research project between Trina Solar and SERIS.

References

[1] A. Fell, "A free and fast three-dimensional/two-dimensional solar cell simulator featuring conductive boundary and quasi-neutrality approximations," *IEEE Trans. Electron Devices*, vol. 60, no. 2, pp. 733–738, Feb. 2013.

[2] R. Brendel, "Modeling solar cells with the dopant-diffused layers treated as conductive boundaries," *Progress Photovoltaics: Res. Appl.*, vol. 20, pp. 31–43, 2012.

[3] A. Cuevas and R. A. Sinton, "Detailed modelling of silicon solar cells," presented at the 23rd Eur. Photovoltaic Sol. Energy Conf., Valencia, Spain, 2008.

[4] A. Cuevas, "Physical model of back line-contact front-junction solar cells," *J. Appl. Phys.*, vol. 113, pp. 164502-1–164502-12, 2013.

[5] A. Cuevas, "Electrons and holes in solar cells with partial rear contacts," *Progress Photovoltaics: Res. Appl.*, 2013. DOI: 10.1002/pip.2433.

[6] P. A. Basore and K. Cabanas-Holmen, "PC2D: A circular-reference spreadsheet solar cell device simulator," *IEEE J. Photovoltaics*, vol. 1, no. 1, pp. 72–77, Jul. 2011.

[7] A. Fell, K. R. McIntosh, M. Abbott, and D. Walter, "Quokka version 2: Selective surface doping, luminescence modeling and data fitting," presented at the 23rd Photovoltaic Sci. Eng. Conf., Taipei, Taiwan, 2013.

[8] P. P. Altermatt, G. Heiser, and M. A. Green, "Numerical quantification and minimization of perimeter losses in high-efficiency silicon solar cells," *Progress Photovoltaics: Res. Appl.*, vol. 4, pp. 355–367, 1996.

[9] S. Kluska, F. Granek, M. Rüdiger, M. Hermle, and S. W. Glunz, "Modeling and optimization study of industrial n-type high-efficiency back-contact back-junction silicon solar cells," *Sol. Energy Mater. Sol. Cells*, vol. 94, pp. 568–577, 2010.

[10] R. Woehl, M. Rüdiger, D. Biro, and J. Wilde, "All-screen-printed back-contact back-junction silicon solar cells with aluminum-alloyed emitter and demonstration of interconnection of point-shaped metalized contacts," *Progress Photovoltaics: Res. Appl.*, 2013. DOI: 10.1002/pip.2418.

[11] O. Nichiporuk, A. Kaminski, M. Lemiti, A. Fave, and V. Skryshevsky, "Optimisation of interdigitated back contacts solar cells by two-dimensional numerical simulation," *Sol. Energy Mater. Sol. Cells*, vol. 86, pp. 517–526, 2005.

[12] K. R. McIntosh, M. J. Cudzinovic, D. D. Smith, W. P. Mulligan, and R. M. Swanson, "The choice of silicon wafer for the production of low-cost rear-contact solar cells," in *Proc. 3rd World Conf. Photovoltaic Energy Convers.*, 2003, vol. 1, pp. 971–974.

[13] R. Bock, S. Mau, J. Schmidt, and R. Brendel, "Back-junction back-contact n-type silicon solar cells with screen-printed aluminum-alloyed emitter," *Appl. Phys. Lett.*, vol. 96, pp. 263507-1–263507-3, 2010.

[14] F. Haase, S. Eidelloth, R. Horbelt, K. Bothe, E. Garralaga Rojas, and R. Brendel, "Loss analysis of back-contact back-junction thin-film monocrystalline silicon solar cells," *J. Appl. Phys.*, vol. 110, pp. 124510-1–124510-9, 2011.

[15] K. C. Fong, K. Teng, K. R. McIntosh, A. W. Blakers, E. Franklin, N. Zin, and A. Fell, "N+ diffusion and contact optimisation of IBC solar cells,"

presented at the 28th Eur. Photovoltaics Sol. Energy Conf., Paris, France, 2013.

[16] E. Franklin, K. C. Fong, K. R. McIntosh, A. Blakers, K. Teng, D. Wang, S. Ngwe, M. Stocks, E. Wang, N. Grant, A. Fell, Y. Wan, Y. Yang, X. Zhang, Z. Feng, and P. J. Verlinden, "Fabrication and characterisation of a 24.4% efficient interdigitated back contact solar cell," presented at the 29th Eur. Photovoltaics Sol. Energy Conf., Amsterdam, The Netherlands, 2014.

[17] R. Sinton, P. Verlinden, R. Swanson, R. Crane, K. Wickham, and J. Perkins, "Improvements in silicon backside contact solar cells for high-value one-sun applications," in *Proc. 13th Eur. Photovoltaic Sol. Energy Conf.*, Nice, France, 1995, pp. 1586–1589.

[18] R. Brendel, S. Dreissigacker, N. P. Harder, and P. P. Altermatt, "Theory of analyzing free energy losses in solar cells," *Appl. Phys. Lett.*, vol. 93, pp. 173503-1–173503-3, 2008.

[19] N. Zin, A. Blakers, E. Franklin, T. Kho, K. Chern, K. McIntosh, J. Wong, T. Mueller, A. G. Aberle, Y. Yang, X. Zhang, Z. Feng, and Q. Huang, "Laser-assisted shunt removal on high-efficiency silicon solar cells," in *Proc. 27th Eur. Photovoltaic Sol. Energy Conf.*, Frankfurt, Germany, 2012, pp. 552–556.

[20] N. Zin, A. Blakers, K. R. McIntosh, E. Franklin, T. Kho, K. Chern, J. Wong, T. Mueller, A. G. Aberle, Y. Yang, X. Zhang, Z. Feng, Q. Huang, and P. J. Verlinden, "Continued development of all-back-contact silicon wafer solar cells at ANU," *Energy Procedia*, vol. 33, pp. 50–63 , 2013. (Proc. PV Asia Pacific Conf., 2012).

[21] K. R. McIntosh and S. C. Baker-Finch, "OPAL 2: Rapid optical simulation of silicon solar cells," in *Proc. IEEE 38th Photovoltaic Spec. Conf.*, 2012, pp. 000265–000271.

[22] P. Campbell and M. A. Green, "Light trapping properties of pyramidally textured surfaces," *J. Appl. Phys.*, vol. 62, pp. 243–249, 1987.

[23] K. R. McIntosh, "Lumps, humps and bumps: Three detrimental effects in the current-voltage curve of silicon solar cells," Ph.D. disertation, Univ. New South Wales, 2001.

[24] K. R. McIntosh and P. P. Altermatt, "A freeware 1D emitter model for silicon solar cells," in *Proc. IEEE 35th Photovoltaic Spec. Conf.*, 2010, pp. 002188–002193.

[25] K. R. McIntosh, P. P. Altermatt, T. Ratcliff, K. C. Fong, L. E. Black, S. C. Baker-Finch, and M. D. Abbott, "An examination of three common assumption used to simulate recombination in heavily doped silicon," in *Proc. 28th Eur. Photovoltaic Sol. Energy Conf.*, Paris, France, 2013, pp. 1672–1679.

Authors' photographs and biographies not available at the time of publication.